2006-04-20

Multiwavelength Observations Of The Blazar Markarian 421 In 2002 December And 2003 January

P. T. Reynolds
Cork Institute of Technology

VERITAS

Recommended Citation

Rebillot, P.F. et al., 2006. Multiwavelength Observations of the Blazar Markarian 421 in 2002 December and 2003 January. The Astrophysical Journal, 641(2), pp.740–751. Available at: http://dx.doi.org/10.1086/500653.

The Astrophysical Journal, 641:740–751, 2006 April 20

MULTIWAVELENGTH OBSERVATIONS OF THE BLAZAR MARKARIAN 421 IN 2002 DECEMBER AND 2003 JANUARY

P. F. Rebillot,[1] H. M. Badran,[2] G. Blaylock,[3] S. M. Bradbury,[4] J. H. Buckley,[1] D. A. Carter-Lewis,[5] O. Celik,[6] Y. C. Chow,[6] P. Cogan,[7] W. Cui,[8] M. Daniel,[7] C. Duke,[9] A. Falcone,[8] S. J. Fegan,[6] J. P. Finley,[8] L. F. Fortson,[10,11] G. H. Gillanders,[7] J. Grube,[4] K. Gutierrez,[1] G. Gyuk,[10,11] D. Hanna,[12] J. Holder,[4] D. Horan,[13] S. B. Hughes,[1] G. E. Kenny,[7] M. Kertzman,[14] D. Kieda,[15] J. Kildea,[12] K. Kosack,[1] H. Krawczynski,[1] F. Krennrich,[5] M. J. Lang,[7] S. Le Bohec,[15] E. Linton,[16] G. Maier,[4] P. Moriarty,[17] J. Perkins,[1] M. Pohl,[5] J. Quinn,[7] K. Ragan,[12] P. T. Reynolds,[18] H. J. Rose,[4] M. Schroedter,[5,13] G. H. Sembroski,[8] G. Steele,[11] S. P. Swordy,[16] L. Valcarcel,[12] V. V. Vassiliev,[6] S. P. Wakely,[16] T. C. Weekes,[13] and J. Zweerink[6] (The VERITAS Collaboration)

and

M. Aller,[19] H. Aller,[19] P. Boltwood,[20] I. Jung,[1] D. Kranich,[21] K. Nilsson,[22] M. Pasanen,[22] A. Sadun,[23] and A. Sillanpaa,[22]

Received 2005 August 22; accepted 2005 December 22

ABSTRACT

We report on a multiwavelength campaign on the TeV γ-ray blazar Mrk 421 performed during 2002 December and 2003 January. These target of opportunity observations were initiated by the detection of X-ray and TeV γ-ray flares with the All Sky Monitor (ASM) on board the *Rossi X-Ray Timing Explorer* (*RXTE*) and the 10 m Whipple γ-ray telescope. The campaign included observational coverage in the radio (University of Michigan Radio Astronomy Observatory), optical (Boltwood, La Palma KVA 0.6 m; WIYN 0.9 m), X-ray (*RXTE* pointed telescopes), and TeV γ-ray (Whipple and HEGRA) bands. At TeV energies, the observations revealed several flares at intermediate flux levels, peaking between 1 and 1.5 times the flux from the Crab Nebula. While the time-averaged spectrum can be fitted with a single power law of photon index $\Gamma = 2.8$ from $dN_\gamma/dE \propto E^{-\Gamma}$, we find some evidence for spectral variability. Confirming earlier results, the campaign reveals a rather loose correlation between the X-ray and TeV γ-ray fluxes. In one case, a very strong X-ray flare is not accompanied by a comparable TeV γ-ray flare. Although the source flux was variable in the optical and radio bands, the sparse sampling of the optical and radio light curves does not allow us to study the correlation properties in detail. We present a simple analysis of the data with a synchrotron self-Compton model, emphasizing that models with very high Doppler factors and low magnetic fields can describe the data.

Subject headings: BL Lacertae objects: individual (Mrk 421) — galaxies: jets — gamma rays: observations — radiation mechanisms: nonthermal — X-rays: individual (Mrk 421)

1. INTRODUCTION

The space-borne EGRET detector on board the *Compton Gamma-Ray Observatory* discovered strong MeV and GeV γ-ray emission from 66 blazars, mainly from flat-spectrum radio quasars and unidentified flat-spectrum radio sources (Hartman et al. 1992, 1999). Ground-based Cerenkov telescopes discovered TeV γ-ray emission from seven blazars, five of which were not detected by EGRET (Horan & Weekes 2004; Aharonian et al. 2005). Although γ-ray emission from blazars has been studied for more than a decade now, it is still unclear where and how the emission originates. According to the most common paradigm, the emission originates close to a mass-accreting supermassive black hole, in a relativistically moving collimated plasma outflow (jet) that is aligned with the line of sight to within a few degrees. The relativistic Doppler effect can explain the intensity of the blazar emission and its rapid variability at X-ray and γ-ray energies on hour timescales: for emission originating from synchrotron or synchrotron self-Compton (SSC) models, the apparent luminosity increases approximately as the fourth power of the relativistic Doppler

[1] Department of Physics, Washington University, St. Louis, MO 63130; rebillot@physics.wustl.edu, krawcz@wuphys.wustl.edu.
[2] Physics Department, Tanta University, Tanta, Egypt.
[3] Department of Physics, University of Massachussetts, Amherst, MA 01003-4525.
[4] School of Physics and Astronomy, University of Leeds, Leeds LS2 9JT, Yorkshire, England, UK.
[5] Department of Physics and Astronomy, Iowa State University, Ames, IA 50011-3160.
[6] Department of Physics, University of California, Los Angeles, CA 90095-1562.
[7] Department of Physics, National University of Ireland, Galway, Ireland.
[8] Department of Physics, Purdue University, West Lafayette, IN 47907.
[9] Department of Physics, Grinnell College, Grinnell, IA 50112-1690.
[10] Department of Astronomy and Astrophysics, University of Chicago, Chicago, IL 60637.
[11] Astronomy Department, Adler Planetarium and Astronomy Museum, Chicago, IL 60605.
[12] Physics Department, McGill University, Montreal, QC H3A 2T8, Canada.
[13] Fred Lawrence Whipple Observatory, Harvard-Smithsonian Center for Astrophysics, P.O. Box 97, Amado, AZ 85645-0097.
[14] Department of Physics and Astronomy, DePauw University, Greencastle, IN 46135-0037.
[15] High Energy Astrophysics Institute, University of Utah, Salt Lake City, UT 84112.
[16] Enrico Fermi Institute, University of Chicago, Chicago, IL 60637.
[17] School of Science, Galway-Mayo Institute of Technology, Galway, Ireland.
[18] Department of Applied Physics and Instrumentation, Cork Institute of Technology, Cork, Ireland.
[19] University of Michigan, Ann Arbor, MI 48109.
[20] Boltwood Observatory, Ontario, Canada.
[21] University of California, Davis, CA 95616.
[22] Tuorla Observatory, FL-21500 Piikio, Finland.
[23] Department of Physics, University of Colorado at Denver and Health Sciences Center, Denver, CO 80208.

factor[24] δ_j, and the observed flux variability timescale is inversely proportional to δ_j.

Blazars are powerful sources across the electromagnetic spectrum. Typical spectral energy distributions (SEDs) for the high-energy peaked TeV blazars show two broad peaks, one at infrared to X-ray energies and the other at X-ray to γ-ray energies. The low-energy peak is commonly believed to originate as synchrotron emission from a population of relativistic electrons gyrating in the magnetic field of the jet plasma. The origin of the high-energy peak is unproven. The commonly adopted and best-studied models assume that the γ-rays are produced in inverse Compton processes by the same electrons that emit the synchrotron radiation at longer wavelengths (for a recent review of observations and models, see Krawczynski 2004). In so-called hadronic models, γ-rays are emitted as synchrotron radiation of extremely energetic protons (Aharonian 2000; Mücke et al. 2003), as inverse Compton and synchrotron emission from a proton-induced cascade (PIC; Mannheim 1998), or from $\pi^0 \rightarrow \gamma\gamma$ decays following the interaction of high-energy protons with some target material (Pohl & Schlickeiser 2000). Recent reviews on observations of blazars with TeV emission and models developed to describe the data can be found in various review articles and books (Krawczynski 2004, 2005; Tavecchio 2006; Weekes 2003; Aharonian 2004). Reviews focussing on observations and models of sources with MeV/GeV emission can be found in Sikora & Madejski (2001) and Coppi (1999). Broader overviews of the field of TeV γ-ray astronomy are given in Buckley et al. (2002), Ong (2003), Weekes (2003), and Aharonian (2004).

Multiwavelength observations are key for understanding the blazar phenomenon. The acquisition of good multiwavelength data sets has encountered substantial difficulties as the sensitivities of current TeV observatories require flares for sampling the TeV light curves on a timescale of hours. Some sources were observed with excellent multiwavelength coverage but during relatively unspectacular quiescent phases; in other cases, the sources were flaring, but the fluxes were only poorly sampled in frequency space and in time. The most remarkable result from the multiwavelength campaigns is that there is good evidence for a correlation between the X-ray fluxes and the TeV γ-ray fluxes for the two sources Mrk 421 (Buckley et al. 1996; Takahashi et al. 1996, 2000; Blazejowski et al. 2005) and Mrk 501 (Djannati-Atai et al. 1999; Sambruna et al. 2000; Krawczynski et al. 2002).

In this paper we present results from a multiwavelength campaign on the TeV blazar Mrk 421. The source is a nearby ($z = 0.031$) high-energy-peaked BL Lac object and was the first extragalactic source detected in the TeV γ-ray band (Punch et al. 1992).

In 2002 November, γ-ray observations with the Whipple 10 m telescope revealed several Mrk 421 flares with fluxes exceeding 3 times the steady flux from the Crab Nebula. The All-Sky Monitor (ASM) instrument aboard *RXTE* also showed extremely strong 2–12 keV fluxes reaching 100 millicrab. Collectively, these triggered a coordinated campaign. We invoked radio, optical, and X-Ray (*RXTE*) observations to commence as soon as the waning moon would allow the Cerenkov telescope to take data once more. Although the X-ray and TeV γ-ray fluxes had decreased substantially when the campaign started on December 4, we acquired a data set with a high signal-to-noise ratio (S/N) X-ray light curve and X-ray energy spectra, and good S/N TeV light curves and TeV γ-ray energy spectra. The combined data allowed us to study the X-ray/TeV γ-ray flux correlation over several weeks. Following our previous study (Blazejowski et al. 2005), this is the second campaign that measures the X-ray/TeV γ-ray flux correlation over several weeks. For the first time, we use here simulated light curves to address the statistical significance of the X-ray/TeV γ-ray flux correlation and to constrain the time lag between the two light curves. Simulations that are necessary as subsequent data points in the light curve are not independent of each other (see, e.g., the discussion by Edelson et al. 1988). The rest of the paper is organized as follows. After describing the data sets in § 2, we explain the method that we used to reconstruct TeV γ-ray energy spectra from the Whipple data and give the results obtained with the method in § 3. Subsequently, we present the results of the campaign in § 4 and conclude with a summary and a discussion in § 5. If not mentioned otherwise, errors are quoted on the level of 1 standard deviation, and upper limits are given at 90% confidence level.

[24] The relativistic Doppler factor is given by $\delta_j = [\Gamma(1 - \beta\cos\theta)]^{-1}$ with Γ, the bulk Lorentz factor of the jet plasma, θ, the angle between jet axis and the line of sight, and β, the plasma velocity, in units of the speed of light.

2. OBSERVATIONS AND STANDARD DATA REDUCTION

2.1. *Radio Observations*

We used the University of Michigan equatorially mounted 26 m paraboloid in its automatic observation mode to observe Mrk 421 at 4.8, 8.0, and 14.5 GHz between 2002 December 3 and 2003 January 10. Both linear polarization and total flux density measurements were made, but only the total flux density measurements are reported here. Each observation consisted of a series of 5 minute ON-OFF type measurements over a 40 minute time period interleaved with observations of other program sources. Observations were restricted to within 3 hr of the local meridian to minimize instrumental errors. The telescope pointing corrections are interpolated from position scans through sources stronger than 2 Jy. The flux density measurements have been corrected to the Baars flux density calibration scale (Baars et al. 1977) using observations of a grid of calibrator sources, distributed around the sky, which were observed at approximately 2 hr intervals. The 1 σ error bars include both the estimated measurement and calibration uncertainties. The observation and calibration procedures have been described in more detail elsewhere (Aller et al. 1985).

2.2. *Optical Observations*

In the following, we discuss three optical data sets. The first was taken at the Boltwood Observatory (Stittsville, Ontario, Canada) with a 0.4 m telescope, a SiTe 502A CCD chip, and a Johnson-Cousins *R* filter. The data were collected for $\sim$ 10 days between 2002 December 3 and 2003 January 12. Relative aperture photometry was performed with an aperture of 10″ and using "star 1" from Villata et al. (1998) as the comparison star. The background was estimated using a concentric annulus with a diameter between 37″ and 44″. We did not subtract the light from the host galaxy. Usually, five 2 minute exposures were integrated before deriving the photometric value. The typical statistical error on the relative photometry is 0.02 mag. The analysis is compromised by two very bright stars near Mrk 421 that cause a varying level of light to spill into the source and background regions. Based on previous optical results on the same source and stars in the field of view, we estimate that photometric measurements have a systematic error of 0.08 mag per data point.

The second set of optical observations was made using a 35 cm Celestron telescope installed on the tube of the 60 cm KVA telescope (La Palma, Spain). The observations were made with the ST-8 CCD using a standard Kron/Cousins *R*-filter. The analysis used the reduction programs developed by Kari Nilsson (Tuorla

Observatory) with the reference stars one and two from Villata et al. (1998).

The final set of optical data were collected using the Wisconsin Indiana Yale NOAO (WIYN) 0.9 m telescope at Kitt Peak National Observatory (KPNO) with the S2KB CCD imager using a Harris *V*-filter. The data were collected from 2002 December 6 to 2003 January 15 (with, however, a large gap 2002 December 9 to 2003 January 3). Relative aperture photometry was performed using standard IRAF routines with an aperture of 6″, sky annulus ranging from 27″ to 30″ in diameter, and star 1 of Villata et al. (1998) as the comparison star. Again, we did not subtract light from the host galaxy. Typical statistical errors from the photometric fits were smaller than 0.005 mag. Using the spread in magnitude difference between two reference stars, we estimate the uncertainty for each data point to be 0.02 mag for the purpose of determining variability. With regard to the absolute flux, due to the presence of host-galaxy light, we expect the values reported to contain an undetermined systematic offset of as much as 0.1 mag. Optical magnitudes for all three data sets are converted to absolute fluxes according to Allen (1973).

2.3. *X-Ray Observations*

We reduced the data from the *RXTE* Proportional Counter Array with the standard *RXTE* data analysis software. Standard-2 mode PCA data taken with the top layer of the operational proportional counter units (PCUs) were analyzed. The number of PCUs operational during a pointing varied between 2 and 4. We restricted the spectral analysis to the energy range from 4 to 15 keV. We excluded data below 4 keV, as the analysis of earlier *RXTE* data showed corrupted behavior (exceptionally high or low count rates of individual bins not compatible with the energy resolution of the instrument). We find that the data of most pointings are dominated by background above 15 keV. After applying the standard screening criteria (including visual inspection of the electron rate) and removing abnormal data spikes, the net exposure in each Good Time Interval ranged from 168 s to 9.01 ks. Light curves were then extracted with FTOOLS version 5.3.2. Background models were generated with the tool `pcabackest`, based on the *RXTE* GOF calibration files for a "bright" source (more than 40 counts s^{-1} PCU^{-1}). Response matrices for the PCA data were created with the script `pcarsp` version 10.1. The PCU "PCU0" was not excluded for analysis as the FTOOLS version gives the proper background model. We assume for all fits a galactic neutral hydrogen density of 1.31×10^{20} cm^{-2} (Dickey & Lockman 1990).[25] For each pointing, a power-law model was fitted over the energy range from 4 to 15 keV.

We complement the data from the pointed *RXTE* telescopes with data from the *RXTE* ASM (Levine et al. 1996) taken between 2002 December 2 (UT) and 2003 January 14 (UT). We derived fluxes by averaging the "summed band intensities" acquired during 1 day.

2.4. TeV γ-*Ray Observations*

TeV observations were taken with the Whipple 10 m Cerenkov telescope (Mount Hopkins, AZ) and with the CT1 telescope of the High Energy Gamma-Ray Astronomy (HEGRA) collaboration (La Palma, Spain). In the following paragraphs we describe the two data sets.

The Whipple observations were taken between 2002 December 4 (UT) and 2003 January 15 (UT). A total of 44 hr of data were acquired: 32 hr on the source, and 12 hr on an adjacent field for background estimation purposes. The data were analyzed using the standard "Hillas" second-moment-parameterization technique (Hillas 1985). Standard cuts (SuperCuts 2000) were used to select γ-ray events and to suppress background cosmic-ray events (de la Calle Perez et al. 2003). The fluxes were normalized to the flux from the Crab Nebula using a data set of 15 hr of on-source data and matching background observations taken in 2002 December and 2003 January (Punch et al. 1991). Using the zenith angle dependence of this Crab data set we account for the zenith angle dependence of the γ-ray excess rate by normalizing our measured Mrk 421 rate to the Crab rate at a corresponding zenith angle. Significances and corresponding error bars were calculated using the method of Li & Ma (1983).

From Monte Carlo simulations, we fold the Crab spectrum with the instrument response to obtain the peak energy (energy threshold) for the Whipple 10 m data to be consistent with the value 400 GeV derived elsewhere (Petry et al. 2002). More detailed descriptions of Whipple observing modes and analysis procedures can be found elsewhere (Weekes 1996; Punch & Fegan 1991; Reynolds et al. 1993). Details about the Whipple telescope including the GRANITE-III camera have been given in Finley et al. (2001).

A second TeV γ-ray data set was acquired with the HEGRA CT1 telescope (see Rauterberg [1995] for a description of the CT1 instrument) between 2002 November 3 and 2002 December 12. The telescope was equipped with a 127 pixel camera with a 3° diameter field of view, and with all-aluminum mirrors giving a total of 10 m^2 reflecting surface (Mirzoyan et al. 1994). The analysis used 17 hr of data with zenith angles between 12° and 58°. The HEGRA CT1 data were normalized to the Crab flux in a similar way as the Whipple data, taking into account the zenith angle dependence of the excess rate. We estimate a mean energy threshold for the CT1 data set of approximately 700 GeV.

The normalization to the steady Crab flux is a convenient way to combine data from different instruments to avoid systematic errors resulting from errors in the absolute flux calibration of each instrument, and to perform a first-order correction for variations in rate with zenith angle. The drawback of the method is that the different energy thresholds of the Whipple and HEGRA observations can introduce a normalization error if the source energy spectrum deviates from the Crab energy spectrum. Using previous measurements of the Mrk 421 TeV spectral index as a function of flux level, we estimate that the Whipple/HEGRA normalization error is always smaller than 30%.

3. DETERMINATION OF TeV γ-RAY ENERGY SPECTRA WITH THE FORWARD-FOLDING METHOD

The spectral analysis of the Whipple TeV γ-ray data used a different set of gamma-hadron separation cuts that minimize the systematic error associated with uncertainties in the γ-ray selection efficiency of the cuts while still giving a good sensitivity. The "extended zenith angle scaled cuts" (Kosack et al. 2004) select primary γ-rays with an efficiency that is largely independent of the zenith angle of the observation and the energy of the primary photon. The analysis is based on the Grinnell-ISU (GrISU) package[26] that uses the KASCADE airshower simulation code (Kertzman & Sembroski 1994), followed by the simulation of the Cerenkov light emitted by the air shower and the simulation of the detector response. To calibrate the overall gain of the Whipple 10 m telescope in the simulations, we compared simulated and observed muon events. Muons show up as bright arcs of Cerenkov light in the camera and are useful for calibration because the light per unit arc length is nearly constant, regardless

[25] See http://asc.harvard.edu/toolkit/colden.jsp.

[26] See http://www.physics.utah.edu/gammaray/GrISU.

TABLE 1
PARAMETERS USED FOR THE TeV γ-RAY ENERGY ESTIMATOR

Parameter	Value
A	−7.05
B	1.30
C	−0.034
D_1	0.057
α	−0.20
D_2	−1.96
β	2.44
d_0 (deg)	0.75

of the impact parameter and angle of the muon trajectory. The overall gain of the telescope can be found by comparing the distribution of the signal per arc length in a simulated set of muon events and in an observed set. We took the simulated muon events from a sample of simulated proton and helium showers. Muons are identified with a dedicated muon identification algorithm that extracts ~200 muon arcs per 28 minute data run. We adjusted the overall gain factor in the simulations until they reproduced the observed signal per arc length distribution. The overall gain factor agrees to within 15% with the value computed from measurements of the mirror reflectivity, photomultiplier tube quantum efficiency, and electronic gain.

We used the forward-folding technique to fit the energy spectra. Although earlier TeV γ-ray analyses used similar methods, this is the first time that we describe the method in detail. For each Cerenkov event that passed the gamma-hadron separation cuts, we computed an estimator E of its primary energy, based on the image parameters size S (sum of counts in an image) and distance d (distance of the image centroid from the center of the field of view):

$$\ln E = g(x) + h(d), \tag{1}$$

with $x = \ln S$, $g(x) = A + Bx + Cx^2$, and $h(d) = D_1 + \alpha d$ for $d < d_0$ and $h(d) = D_2 + \beta d$ for $d > d_0$. The constants A, B, C, D_1, D_2, α, β, and d_0 are given in Table 1. The first term in the energy estimator reflects the fact that total intensity of an image (*size*) is roughly proportional to the energy (E) of the inducing γ-ray. The second term corrects this relationship depending on the distance of the telescope from the shower axis (d is proportional to the latter). Using extended zenith angle cuts, the energy estimator gives an energy resolution of $\sigma(\ln E) = 0.25$.

We limited the spectral analysis to ON-source data with associated background data sets (the so-called ON-OFF data) taken at zenith angles less than 30°. After histogramming the energy estimator for both the ON-source and background regions, the background histogram was subtracted from the ON-source histogram. Subsequently, an energy spectrum was fitted to this "excess histogram" using the forward-folding approach (see, e.g., Fenimore et al. 1982), making use of a simulated set of γ-ray showers. The simulated set of showers consisted of 67,500 showers simulated over an area $A_{\rm MC} = \pi(400\ {\rm m})^2$ in the energy range from 50 GeV to 25.6 TeV over nine energy intervals. The first energy interval went from 50 to 100 GeV, the second from 100 to 200 GeV, and so forth. In the ith energy interval, showers were simulated according to a power-law distribution:

$$\frac{dN_{\rm MC}^{(i)}}{dE} = N_i(E/1\ {\rm TeV})^{-\Gamma_{\rm MC}} \tag{2}$$

with $\Gamma_{\rm MC} = 2.5$. Simple integration of equation (2) gives the normalization constant N_i as function of the lower bound $E_{{\rm min},i}$ and upper bound $E_{{\rm max},i}$ of the ith energy interval and the number n_i of showers simulated in that energy interval:

$$N_i = \frac{-n_i(-\Gamma_{\rm MC}+1)}{E_{\rm min,i}^{-\Gamma_{\rm MC}+1} - E_{\rm max,i}^{-\Gamma_{\rm MC}+1}}. \tag{3}$$

We fit the data with two models, a power-law model and a power-law model with an exponential high-energy cutoff:

$$\frac{dN_\gamma}{dE} = N_0(E/1\ {\rm TeV})^{-\Gamma} \tag{4}$$

and

$$\frac{dN_\gamma}{dE} = N_0(E/1\ {\rm TeV})^{-\Gamma}\exp(-E/E_0), \tag{5}$$

where N_0 is the flux normalization at 1 TeV, Γ is the photon index, and E_0 is the high-energy cutoff. For each trial parameter set $\mathcal{P}$ (with $\mathcal{P} = \{N_0,\ \Gamma\}$ or $\mathcal{P} = \{N_0,\ \Gamma,\ E_0\}$), another histogram is filled with weighted γ-ray showers that pass the γ-ray selection cuts. The weights are computed according to

$$W_i(E;\ \mathcal{P}) = \frac{\left(dN_\gamma/dE\right)(E;\ \mathcal{P})}{\left(dN_{\rm MC}^{(i)}/dE\right)(A_{\rm MC}\Delta t)^{-1}}, \tag{6}$$

where Δt is the observation time, and $A_{\rm MC}$ is the area over which showers were simulated. The numerator in equation (6) gives the model flux for the parameter combination $\mathcal{P}$ at energy E. The denominator gives the simulated flux. While the weights depend on the true energy of the simulated γ-rays, the showers are filled into the histogram according to their reconstructed energy. The weighting saves computational time in the fitting procedure, as only the weights have to be recomputed for each set of model parameters.

We performed a search in parameter space until the parameter combination $\mathcal{P}_{\rm min}$ is found that minimizes the χ^2-difference between the observed and simulated histograms. We determined the 1 σ error region from the condition

$$\chi^2(\mathcal{P}) \le \chi^2(\mathcal{P}_{\rm min}) + 1 \tag{7}$$

(Press et al. 1992).

The best-fit model parameters and the associated errors are the main results of a spectral analysis. Plotting individual data points in an energy spectrum is well known to be an ill-defined problem. A very good discussion can be found in Loredo & Epstein (1989). Owing to the finite energy resolution of the telescopes, some information about the true energy spectrum is irrevocably lost. We have experimented with "deconvolution methods," as for example, the Backus-Gilbert method (Backus & Gilbert 1970; Loredo & Epstein 1989). Owing to a combination of almost Gaussian distributions of $\ln(E_{\rm true} - E_{\rm rec})$ and $E_{\rm true} - E_{\rm rec}$ and the modest S/Ns of the TeV γ-ray energy spectra, we find that deconvolution methods improve only very little the effective energy resolution.

We thus use the simplest method to plot flux estimates, based on the counts in the excess histogram (see, e.g., Fenimore et al. 1982). For an energy bin stretching from E_1 to E_2, we plot the flux value at the energy $E = 10^{(\log E_1 + \log E_2)/2}$. The flux value is

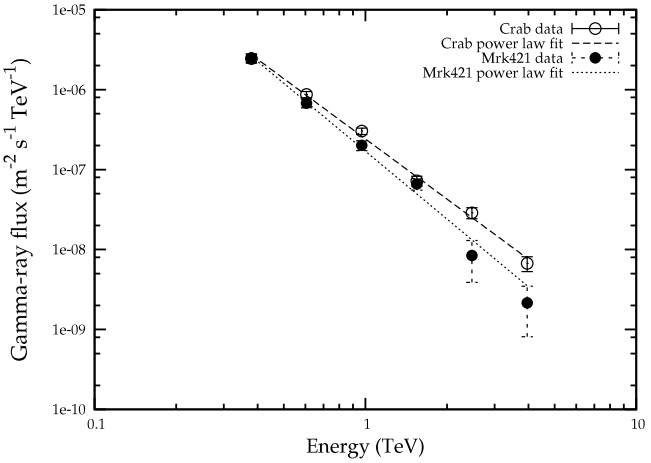

FIG. 1.—Whipple TeV spectrum of the Crab Nebula and Mrk 421. The dashed and dotted lines give the results of power-law fits for the Crab Nebula and Mrk 421, respectively.

given by scaling the best-fit model according to the observed number of excess counts:

$$f = \frac{dN}{dE}(\mathcal{P}_{\min})\frac{k_i}{\langle k_i \rangle}. \quad (8)$$

Here k_i is the number of excess counts in the ith bin of the signal histogram, and $\langle k_i \rangle$ is the sum of weights of the simulated events in the ith bin.

Figure 1 shows the Crab spectrum from small zenith angle data ($<30^{\circ}$) acquired between 2002 September 14 (UT) and 2003 March 24 (UT), and the time -averaged TeV γ-ray spectrum of Mrk 421 for the data set of the multiwavelength campaign. Both data sets are from the Whipple 10 m telescope. The power-law fit to the Crab data gives a flux normalization of $(2.42 \pm 0.11) \times 10^{-11}$ photons cm^{-2} s^{-1} TeV^{-1}, and a photon index of $\Gamma = 2.5 \pm 0.1$. The χ^2 is 5.27 for 4 degrees of freedom.

These results should be compared to previous results. The Whipple collaboration obtained a flux normalization $N_0 = (3.25 \pm 0.14 \pm 0.60) \times 10^{-11}$ photons cm^{-2} s^{-1}, and a spectral index $\Gamma = 2.49 \pm 0.06 \pm 0.04$ (Hillas et al. 1998). The HEGRA collaboration published $N_0 = (2.83 \pm 0.04 \pm 0.60) \times 10^{-11}$ photons cm^{-2} s^{-1}, and $\Gamma = 2.62 \pm 0.02 \pm 0.05$ (Aharonian et al. 2004). Finally, the CAT collaboration obtained $N_0 = (2.21 \pm 0.05 \pm 0.60) \times 10^{-11}$ photons cm^{-2} s^{-1}, and $\Gamma = 2.80 \pm 0.03 \pm 0.06$ (Piron et al. 2001). The first error values are the statistical error values, and the second are the systematic error values (both errors on 1 σ confidence level). The systematic errors on the absolute flux are about 25% and derive from the uncertainty of the energy threshold of the instruments combined with the steep spectrum of the Crab Nebula. Our result derived here lies below the previously published values of Whipple and HEGRA and above the value published by CAT. The discrepancies are comparable to the 1 σ confidence levels. It should be noted that the Whipple results published in 1998 were taken with a significantly different hardware configuration. Furthermore, we relied here on a energy threshold calibration with muons, while Hillas et al. (1998) used the comparison between the detection rate of simulated and observed cosmic rays to calibrate the energy threshold of the telescope. Each calibration method has its own systematic uncertainty, and it is difficult to decide which one is more reliable. The discussion shows that one should consider the full systematic error when comparing the two Whipple results with each other. The three experiments quote a systematic error of $\simeq 0.05$ on the photon index. Here our result agrees well with the previous Whipple measurements; the HEGRA spectrum is somewhat steeper and the CAT spectrum is significantly steeper. The comparison of all four results shows that systematic errors are larger than estimated. In the case of the blazar observations discussed below, the uncertainty of the absolute energy threshold are not that important, as we are mostly interested in relative flux variations. We correct our fluxes with a "throughput factor" derived from the cosmic-ray detection rate measured during each data run to correct for variations in the atmospheric conditions. As cosmic-ray showers are not identical to air showers, we estimate that the systematic uncertainty on diurnal fluxes is 10%, and the systematic error on diurnal photon indices is 0.1.

The power-law fit to the Mrk 421 data gives a flux normalization of $(1.7 \pm 0.1) \times 10^{-11}$ photons cm^{-2} s^{-1} TeV^{-1}, and a photon index of $\Gamma = 2.8 \pm 0.1$. The χ^2 is 5.06 for 4 degrees of freedom. The flux and photon index lie in the range of previous observations (Zweerink et al. 1997; Aharonian et al. 1999; Krennrich et al. 1999, 2002; Krennrich & Dwek 2003). We find that the photon statistics do not allow us to derive meaningful constraints on the high-energy cutoff E_0.

Using the best-fit parameters from the Crab spectral analysis, we can weight the Monte Carlo events by the determined spectrum and compare several simulated distributions of the image parameters with the background subtracted distributions for the Crab data (Fig. 2). The good agreement between simulated and experimental data verifies that the simulations describe the air showers and the detector response adequately.

4. RESULTS FROM THE MULTIWAVELENGTH CAMPAIGN

4.1. *Overview*

Figures 3 and 4 combine all the light curves measured in 2002 December and 2003 January, respectively. From top to bottom, the figures show the TeV γ-ray data, TeV photon indices Γ (where $dN/dE \propto E^{-\Gamma}$), *RXTE* PCU 10 keV flux amplitudes (from the 4–15 keV spectral fits), the 4–15 keV photon indices, the *RXTE* ASM 2–12 keV fluxes, the optical data, and the radio data.

The TeV γ-ray fluxes varied between 0 and $\sim$2 times that of the Crab Nebula, with slightly higher fluxes observed during the second half of the campaign. We determined TeV photon indices on a night to night basis whenever the flux was sufficiently high to warrant a spectral analysis. For epochs of low fluxes (2002 December 6 and 7 (UT) (MJD 52,614–52,615), 2002 December 8, 9, and 10 (UT) (MJD 52,616–52,618), 2002 December 14, 15, and 16 (UT) (MJD 52,622–52,624), and 2003 January 7 and 8 (UT) (MJD 52,646–52,647)) we combined the data of several nights to determine an energy spectrum. A χ^2 test of statistical variability was performed by fitting the entire TeV photon index data set to a constant function. The best fit to the data, with 2 σ errors, is $\Gamma = -2.864 \pm 0.097$, with a χ^2 value of 46.5 for 20 degrees of freedom. The probability of obtaining this value by chance is 2.2×10^{-4}. Seven data points lie outside the 2 σ confidence region.

The 4–15 keV *RXTE* data are shown in Figures 3 and 4. The X-ray fluxes varied between 0.2×10^{-3} and 4.5×10^{-3} counts cm^{-2} s^{-1} keV^{-1}. Strong flares were observed on 2002 December 3 (MJD 52,611), 2002 December 5 (MJD 52,613), 2003 January 10 (MJD 52,649), and on 2003 January 14 (MJD 52,653). The 4–15 keV X-ray photon indices show a large range of values from $\Gamma = 1.97$ to 2.90.

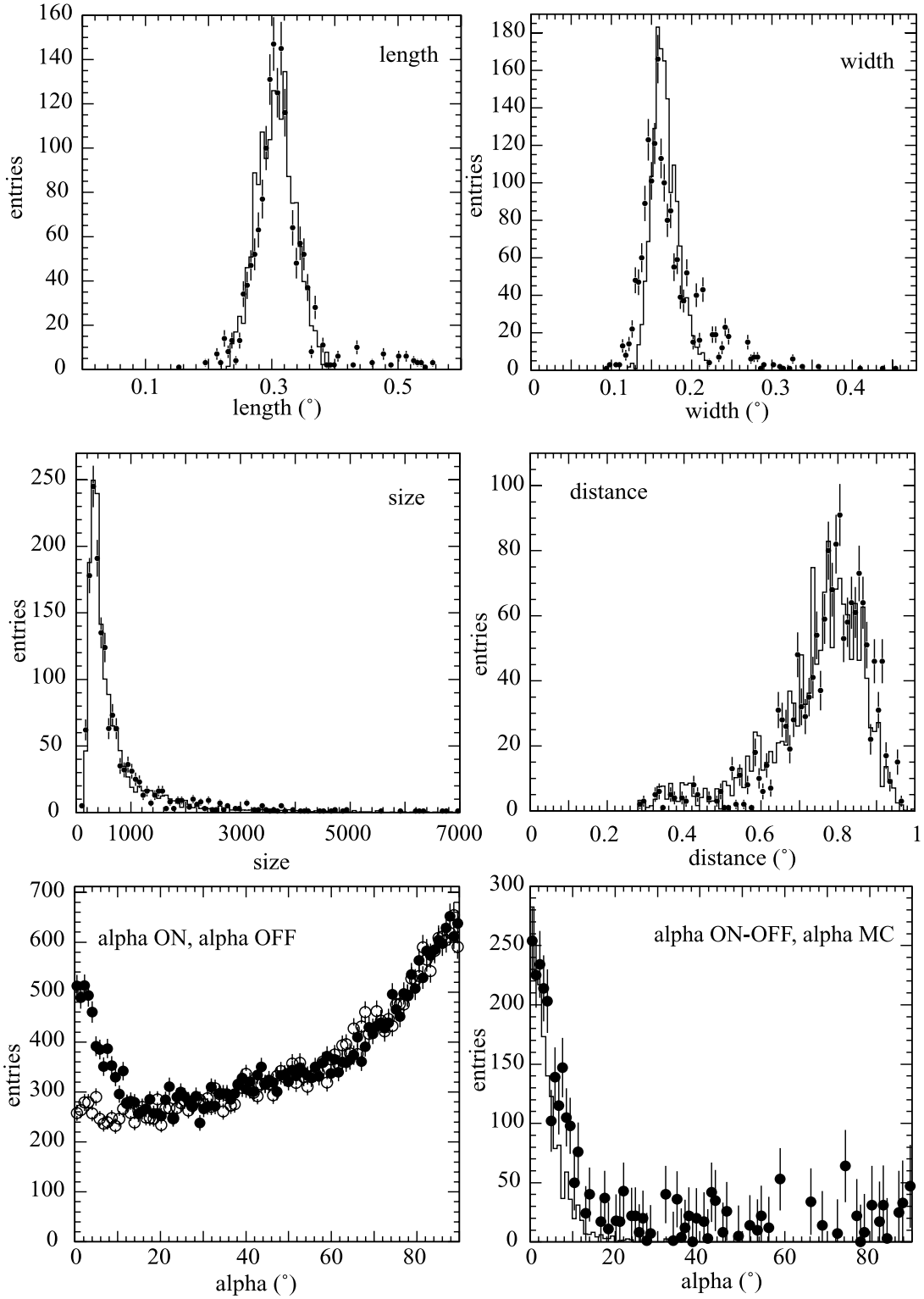

FIG. 2.—Hillas parameter distributions for Whipple 2002–2003 Crab ON/OFF data and simulated data. Histograms show simulated data, while data points show Crab data.

The values of $\Gamma \geq \sim 2$ indicate that the presumed synchrotron SED peaked at and below the 4–15 keV energy range covered by observations. In two cases, the X-ray index varies very rapidly: on MJD 52,619 it changes by $\Delta\Gamma = 0.22$ within 1.4 hr, and on MJD 52,650 it changes by $\Delta\Gamma = 0.14$ within 1.6 hr.

Over the duration of the campaign, the 4–15 keV photon index changed by $\Delta\Gamma \approx 1$. Synchrotron cooling of a power-law distribution of electrons produces a spectral break equal to or smaller than $\Delta\Gamma = 0.5$ if the high-energy cutoff of the electron spectrum is outside the range sampled by the observations. If the power-law index of the accelerated particles does not change with time, the detection of spectral variations with $\Delta\Gamma > 0.5$ thus implies that the 4–15 keV fluxes are influenced by the high-energy cutoff of the relativistic electron population. Alternatively, flares might be associated with changes of several parameters constraining the emitting

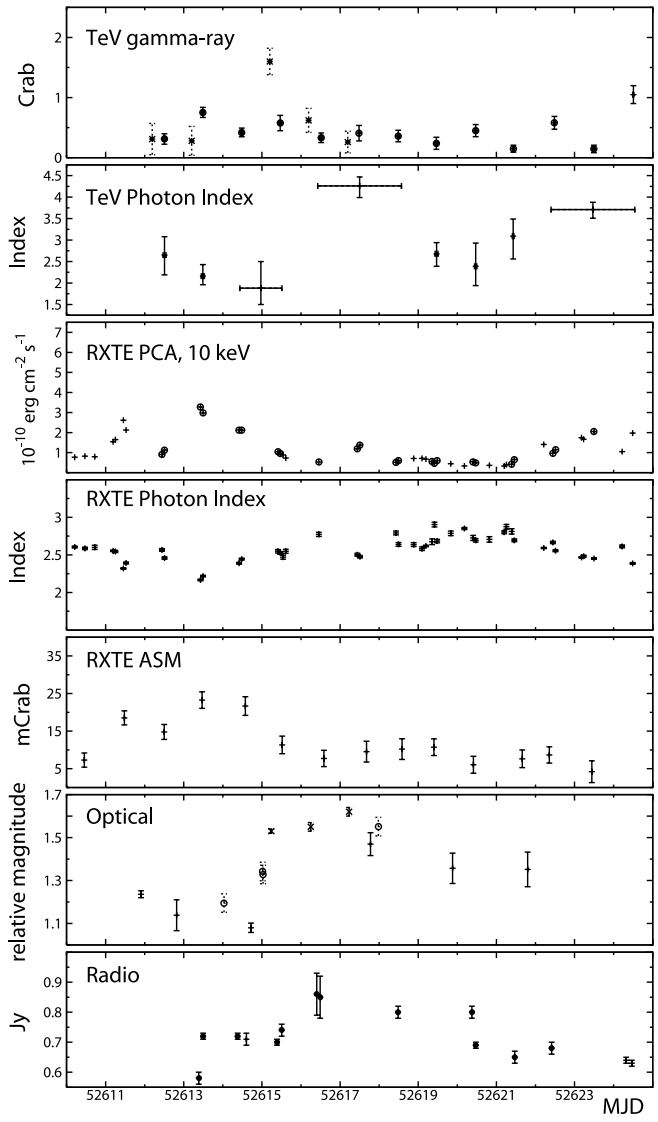

FIG. 3.—Multiwavelength data from 2002 December. The γ-ray data points show per-night averages, in crab units. Starred data points signify data taken from the HEGRA CT1 telescope, while crosses denote Whipple 10 m data. The error bars on the *RXTE* PCA data are not shown as they are smaller than the symbol size, and have units of 10^{-10} ergs cm^{-2} s^{-1} at 10 keV. The circled X-ray and γ-ray data points overlapped or were taken less than 5 minutes apart. The TeV γ-ray and *RXTE* photon indices show Γ, where $dN/dE \propto E^{-\Gamma}$. The ASM data are given in mcrab. In the optical band, open circles show the WIYN *V*-band data, crosses show the Boltwood *R*-band data, and crosses denotes La Palma *R*-band data. All of the optical data are in relative magnitude units. The open (filled) circles in the radio band show measurements that overlapped or were taken within 5 minutes of a TeV γ-ray observation (X-ray and TeV γ-ray observation). The radio data are given in janskys.

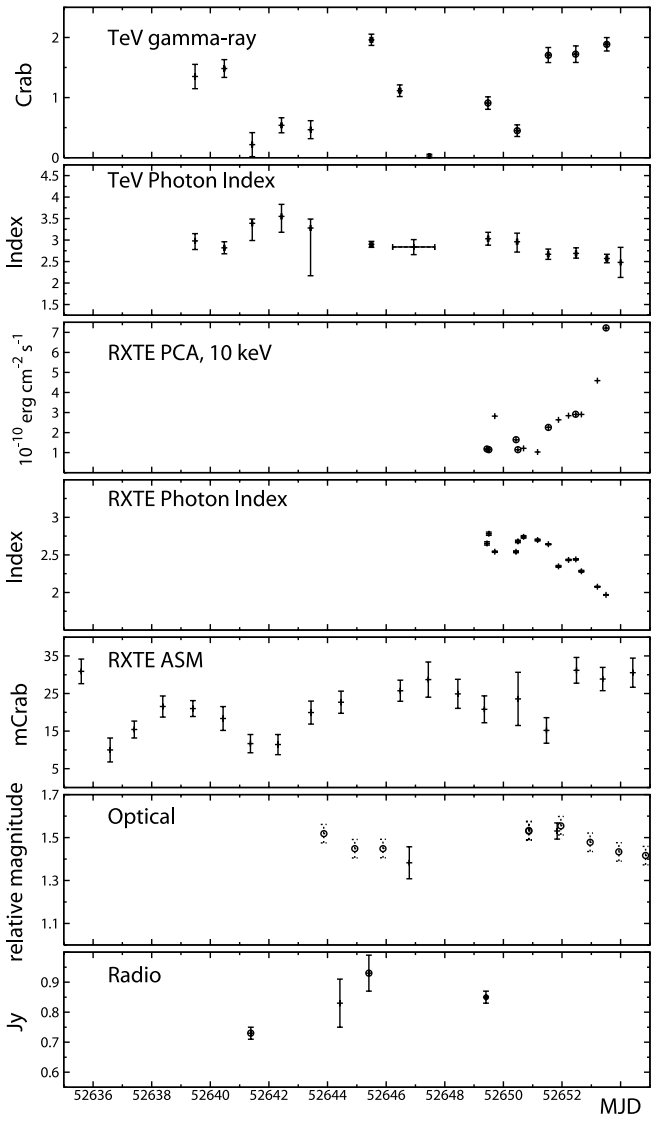

FIG. 4.—Same as Fig. 3, but for the data from 2003 January.

plasma, as for example the jet magnetic field or the jet beaming angle.

The *RXTE* PCU and ASM fluxes seem to trace each other, although the sparse sampling of the PCU data and the large statistical error bars of the ASM data do not allow us to draw definitive conclusions. The optical and radio data show substantial variability by about $\pm 50\%$ of the mean flux, but no detailed correlation is present. This is not a surprise since for the optical data one expects sizeable contributions from the galaxy light and perhaps thermal emission from the accretion disk in addition to optical synchrotron. Furthermore, one expects longer variability timescales for the lower energy synchrotron radiation, since the lower energy electrons that produce this radiation cool more slowly.

4.2. *The X-Ray/TeV γ-Ray Flux Correlation*

We studied the X-ray and TeV γ-ray flux correlation with the help of the discrete correlation function (DCF) of Edelson et al. (1988). The DCF gives the linear correlation coefficient for the two light curves as a function of a time lag between them. The DCF is the standard tool used in the case of sparsely sampled data and gives fewer spurious results than a traditional correlation function analysis that interpolates between light-curve data points. We determined the statistical significance of the correlation coefficients with the help of a set of simulated γ-ray light curves, computing for each simulated light curve the DCF with the observed X-ray data (J. H. Buckley et al. 2006, in preparation). These light curves are generated by a superposition of triangular shots, with all shots having the same amplitude and the same rise and fall time.

Figure 5 gives the DCF for the X-ray and TeV γ-ray data sets. For a time lag of 0 days, we find a DCF value of 0.58 ± 0.12. The simulated data sets show that the correlation is significant. For uncorrelated light curves consisting of triangular shots with the same structure function, we calculate that the chance probability to get a larger DCF value at a time lag of zero days is 3.12%. Figure 6 shows the X-ray/TeV γ-ray flux correlation for all

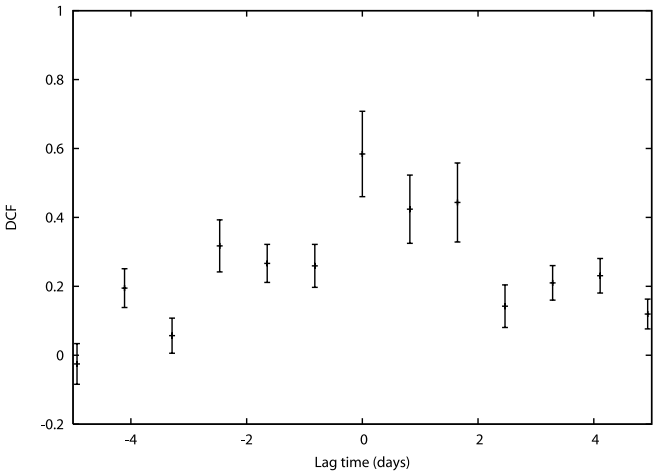

FIG. 5.—Discrete correlation function of the complete X-ray and γ-ray data set. A positive time lag means the γ-ray flux precedes the X-ray flux.

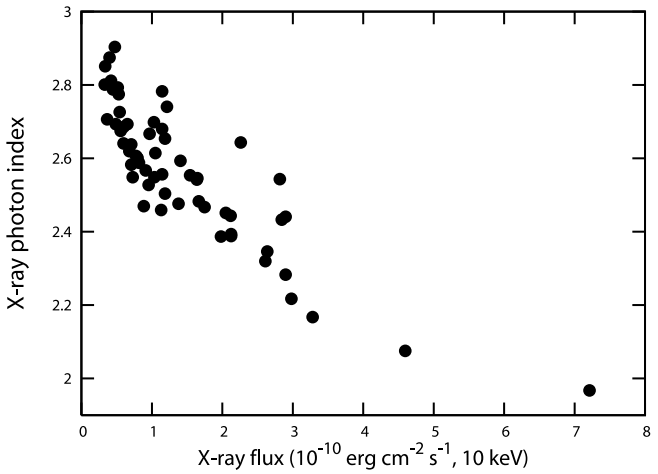

FIG. 7.—Correlation of the 10 keV X-ray flux and the 3–14 keV photon index (both use *RXTE* PCA data).

overlapping observations. The measurements entering this figure are shown by the circled data points in Figures 3 and 4. Each of these overlapping observations are simultaneous to within 5 minutes. The correlation shows substantial scatter, with similar X-ray (TeV) fluxes sometimes corresponding to TeV (X-ray) fluxes that differ by more than a factor of 2 from each other. The scatter may be an inherent property of the emission mechanism. Alternatively, it may be caused by a short time lag between the flares in the two bands, not resolved by the sparse sampling during the campaign.

4.3. *Evolution of the X-Ray Photon Indices*

Figure 7 shows the correlation between the 10 keV fluxes and the 4–15 keV photon indices. A correlation can clearly be recognized in the sense that higher fluxes are accompanied by harder energy spectra. A similar correlation (harder energy spectra for higher fluxes) has been reported for other BL Lac–type objects, e.g., Mrk 501 (Kataoka et al. 1999; Krawczynski et al. 2000), 1ES 1959+650 (Krawczynski et al. 2002), H 1426+428 (Falcone et al. 2004), and PKS 2155−304 (Kataoka et al. 2000).

We further scrutinized the temporal evolution of the photon indices with so-called X-ray hysteresis curves (Takahashi et al. 1996; Kirk & Mastichiadis 1999), plotting the X-ray photon index as a function of X-ray flux, and indicating the temporal sequence of the measurement throughout the evolution of individual flares. In the simplest model whereby flares are formed by short-lived shocks (e.g., internal shocks from colliding blobs), one expects the temporal evolution to be dictated by the interplay of the acceleration, cooling, and confinement times. For the Fermi mechanism, the particle energies reached depend on the allowed acceleration time. Thus, during the beginning of flares, the X-ray and γ-ray energy spectra are expected to harden. Once synchrotron cooling starts to dominate the particle energy spectra, the emitted photon energy spectra are expected to soften. We studied two X-ray flares, one occurring at the beginning of the campaign (MJD 52,612–52,615), and the other at the end (MJD 52,651–52,653). The first flare is shown in Figure 8. This flare coincided with an increase of the TeV γ-ray flux by a factor of 2.4 from MJD 52,612 to 52,613. The X-ray spectrum hardens during the rising phase of the flare and softens during the decaying phase. Furthermore, the X-ray spectrum is softer during the falling phase than during the rising phase. The "clockwise" evolution in the Γ_X-F_X plane is consistent with the expectations from stochastic Fermi acceleration and synchrotron cooling as described above. The data of the second flare are shown in Figure 9. The TeV γ-ray flux increased from MJD 52,650 to 52,651 by a factor of 3.8 and remained roughly constant during the following two nights of observations. While the X-ray flux increased from MJD 52,652 to 52,653 by a factor of $\sim$2.5, the TeV flux measured at the same time as the X-ray fluxes did not increase substantially. The general trend is that the spectrum hardens as the flux increases, although at MJD 52,652.25, the spectrum softens temporarily while the flux is still increasing. Unfortunately, our observations did not cover the decaying phase of the flare.

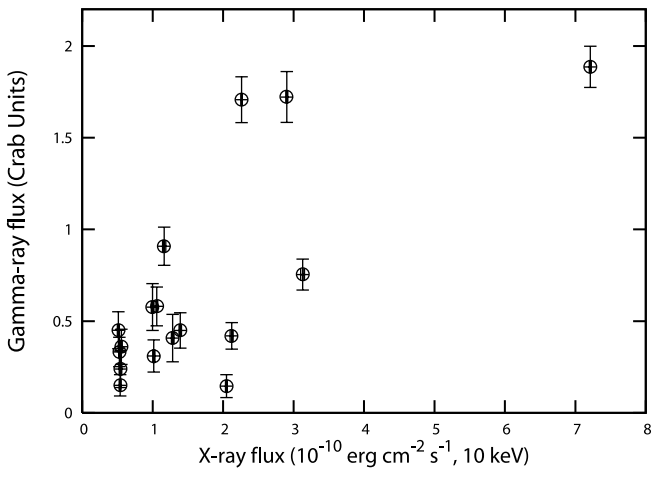

FIG. 6.—Plot of the TeV γ-ray vs. X-ray flux correlation for measurements for all overlapping data sets.

5. DISCUSSION

The multiwavelength campaign showed Mrk 421 in a level of intermediate activity. During the observational campaign, Mrk 421 showed significant flux variability in the radio, optical, X-ray, and γ-ray bands and significant spectral variability at X-rays and TeV γ-rays. While we measured an average TeV γ-ray photon index of $\Gamma = 2.8$, the observations revealed evidence for spectral variability on a timescale of days. In particular, the data suggest very soft energy spectra with $\Gamma \approx 4$ during the first half of the observation campaign. One of the most interesting results from this campaign is that the X-ray and TeV γ-ray fluxes are correlated on the $\sim$97% confidence level, but we find widely different TeV γ-ray fluxes for a single X-ray flux and vice versa.

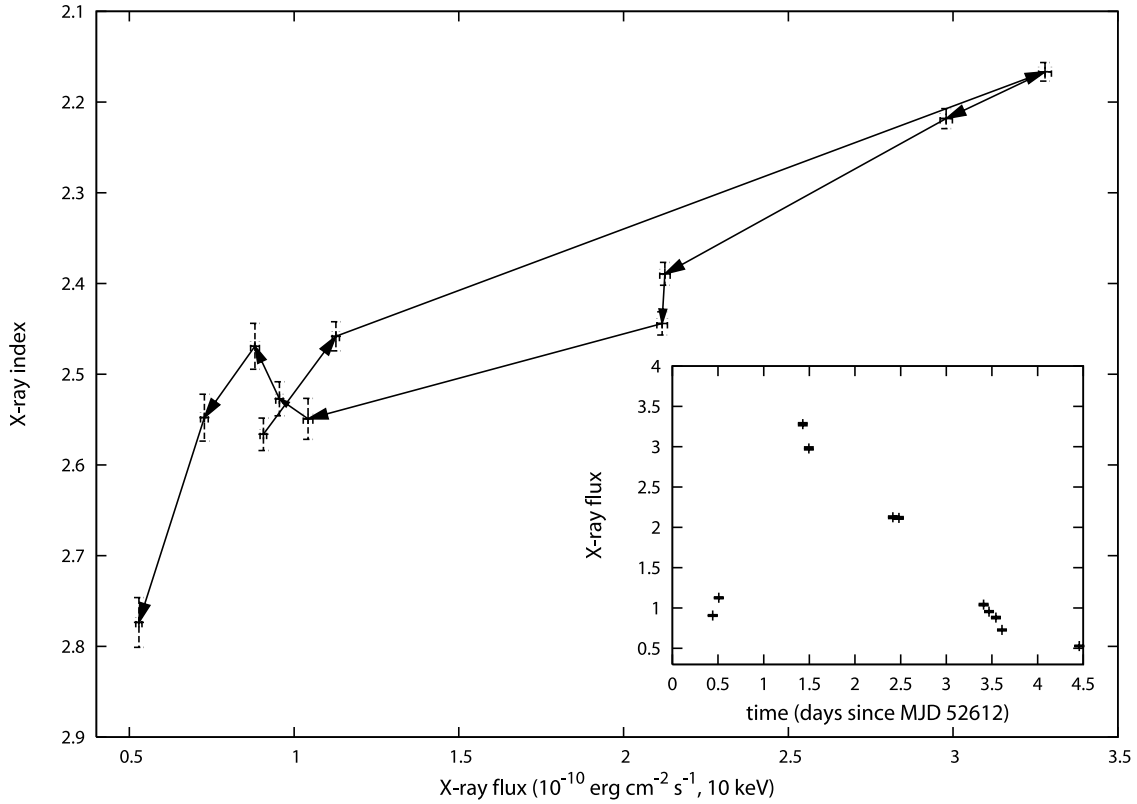

FIG. 8.—X-ray power-law photon index vs. X-ray flux for the MJD 52,612–52,615 X-ray flare.

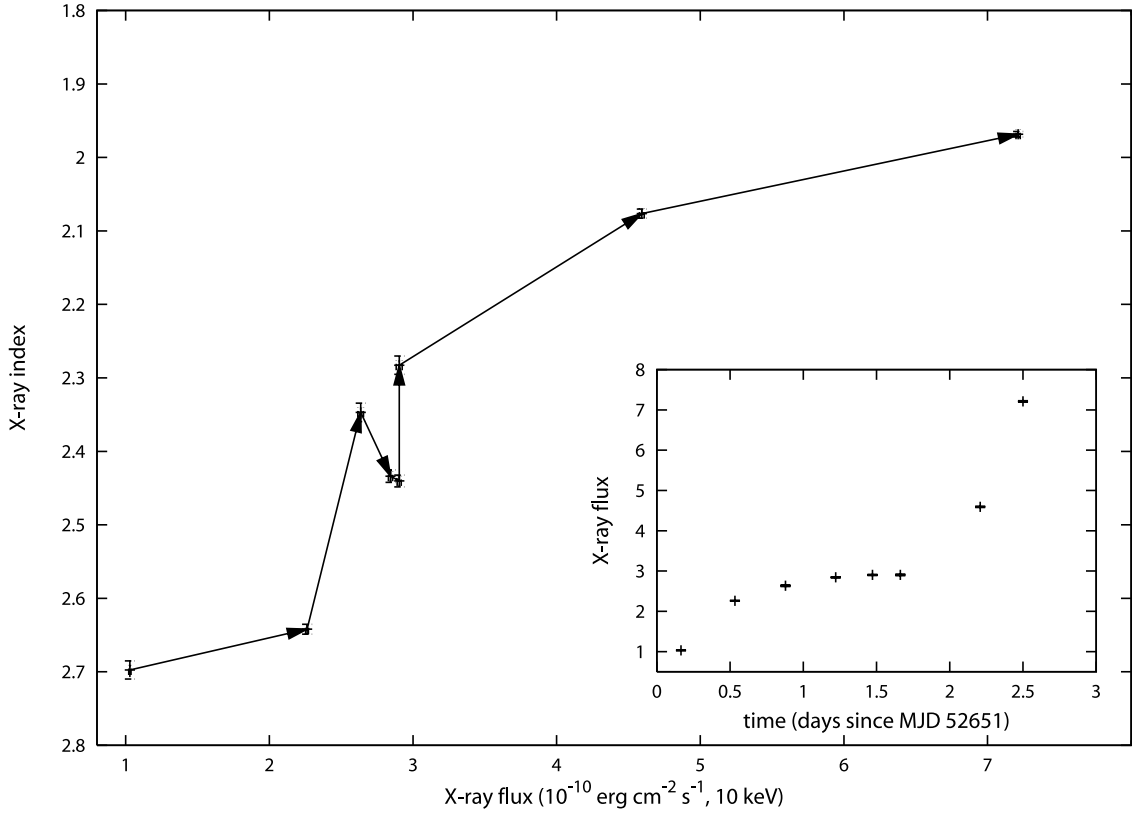

FIG. 9.—X-ray power-law photon index vs. X-ray flux for the MJD 52,651-52,653 X-ray flare.

The most extreme example is the "orphan X-ray flare," seen on 2003 January 13 (MJD 52,653). The loose X-ray/TeV correlation may suggest that the model parameters (e.g., the volume of the emission zone) change with time or that the commonly made assumption of an SSC emission zone is an oversimplification. Our previous observations of Mrk 421 had already shown a rather loose X-Ray/TeV γ-ray correlation (Blazejowski et al. 2005) and the same applied for 1ES 1959+650 (Krawczynski et al. 2004). In the case of Mrk 501, a rather tight correlation has been reported (Krawczynski et al. 2000, 2002).

The analysis of the correlation between the X-ray flux and photon index during a flare indicated a clockwise hysteresis. For Mrk 421, Takahashi et al. (1996) also reported clockwise evolution. However, Takahashi et al. (2000) reported evidence for both, clockwise evolution during some flares and counterclockwise evolution during other flares. If the SSC model indeed applies, these results may imply that the characteristic timescales of the most important processes (acceleration time, radiative cooling time, escape time) change from flare to flare and thus yield the different observed hysteresis behaviors. Recently, Sokolov et al. (2004) emphasized that the geometry of the emitting region and its orientation relative to the line of sight influences the observed flux and spectral evolution and might thus further complicate the interpretation of the results.

The X-ray and TeV γ-ray emission from Mrk 421 data have been modeled with SSC codes by many groups (see, e.g., Inoue & Takahara 1996; Bednarek 1997; Bednarek & Protheroe 1999; Böttcher et al. 1997; Mastichiadis & Kirk 1997; Tanahita et al. 2001; Krawczynski et al. 2001; Konopelko et al. 2003; Kino et al. 2002; Blazejowski et al. 2005). A crucial model parameter is the jet Doppler factor δ_j. The published models with Doppler factors δ_j of 20 or lower generally predict TeV energy spectra that are softer than the observed ones, especially if a correction for extragalactic absorption would be applied that steepens the energy spectra considerably. Models with Doppler factors δ_j on the order of 50 give satisfactory model fits to both the X-ray (synchrotron) and the TeV (inverse Compton) emission (see the self-consistent modeling of Krawczynski et al. [2001] and Konopelko et al. [2003] and the discussions by Tavecchio [2006] and Piner & Edwards [2005]). Piner & Edwards (2005) observed the Mrk 421 parsec-scale radio jet with the Very Large Baseline Array (VLBA). Remarkably, they find apparent pattern speeds of only $\sim 0.1c$. As discussed by the authors, the highly relativistic motion inferred from TeV observations can be reconciled with the modestly relativistic flow calculated from VLBA observations by postulating that the jet slows down between the subparsec (TeV) and parsec (VLBA) regimes.

It may be possible to describe the multiwavelength data with a SSC model and lower Doppler factors by invoking additional seed photons. Two new model variants that combine ingredients of SSC and external Compton models have been proposed by Georganopoulos & Kazanas (2003) and by Ghisellini et al. (2005). While the first authors assume that downstream emission regions provide seed photons, the second authors speculate that the jet is composed of a fast spine with a slow-moving envelope. In this model, the fast spine emits the X-ray and γ-ray radiation. Modeling of the data with these two inhomogeneous models is outside the scope of this paper.

In this discussion we do not want to embark on comprehensive modeling of the data from the entire campaign. Our main aim is to draw the attention of the reader to a single remarkable fact: while it is difficult to model the data with Doppler factors on the order of 20 and lower, much higher Doppler factors cannot be excluded right away. Figure 10 shows two SSC models based on

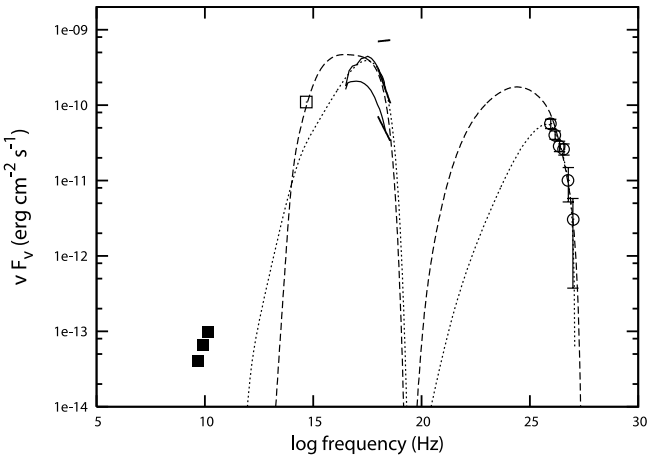

FIG. 10.—Mrk 421 SEDs measured during the campaign. The data points show the radio to γ-ray data. The radio and optical spectra show the average fluxes observed during the campaign. At X-rays we show three spectra, one from the *RXTE* pointing with the highest flux observed during the campaign, one from the pointing with the lowest flux, and one spectrum at intermediate flux levels. The intermediate X-ray spectrum and the gamma-ray spectrum were determined using for both only the data taken during nights with simultaneous X-ray and gamma-ray observations. The solid curved lines show, for comparison, a low-flux and a high-flux energy spectrum measured with *BeppoSAX* (*Beppo Satellite per Astronomia X*) during the 1998 flaring period (Fossati et al. 2000). The long dashed lines show the results from a simple SSC model with $\delta = 1000$, while the short dashed lines show the results with $\delta = 50$.

the simple snapshot code of Krawczynski et al. (2004). The code assumes a single spherical emission volume of radius R relativistically approaching the observer with a jet Doppler factor δ_j. The emission volume is homogeneously filled with a tangled magnetic field of strength B and a nonthermal electron population. The electron energy spectrum follows $dN/d\gamma \propto \gamma^{-p}$ with $p = 2$ for electron Lorentz factor γ between $\gamma_{\rm min}$ and γ_b and $p = 3$ for Lorentz factors between γ_b and $\gamma_{\rm max}$. The code models extragalactic absorption owing to the $\gamma_{\rm TeV} + \gamma_{\rm CIB} \rightarrow e^+e^-$ pair-production processes of TeV photons on photons from the cosmic infrared background (CIB) using the CIB model of Kneiske et al. (2002).

We discuss two models. We show the first model for illustrative purposes only. It uses the "conventional" model parameters ($\delta_j = 50$) derived from the time-dependent self-consistent analysis of a different but similar data set (Krawczynski et al. 2001). The second model uses a very high Doppler factor ($\delta_j = 1000$). All the model parameters are given in Table 2. For both models, we assured that the model parameters were chosen self-consistently. Causality arguments require that the radius R satisfies $R < \delta_j c \Delta T_{\rm obs} = 2.7 \times 10^{15}$ cm for $\delta_j = 50$ and $R < 5.4 \times 10^{16}$ cm for $\delta_j = 1000$ for a flux variability timescale of $\Delta T_{\rm obs} = 30$ min. Note that the flux variability timescale sets a lower limit on R but no upper limit, if the flux variability timescale is not dominated by light travel time effects but by other effects (e.g., by the stability of a strong shock front). We checked that the SED (1) fits the X-ray and TeV γ-ray data and (2) is consistent with the expected spectral shape owing to radiative cooling. In the first model, the latter self-consistency is assured by our previous self-consistent time-dependent modeling. In the second model, we construct an electron spectrum based on the general results for electrons suffering synchrotron and inverse Compton losses (Syrovatskii 1959; Kardashev 1962; Ginzburg & Syrovatskii 1964; Pacholczyk 1970; Inoue & Takahara 1996). We assume that the electron energy spectrum breaks at $\gamma_b = 1.8 \times 10^3$. The laboratory-frame synchrotron cooling time for electrons at the

TABLE 2
PARAMETERS FOR TWO SYNCHROTRON SELF-COMPTON MODELS

δ	B (G)	R (m)	$\log \gamma_{\rm min}$	$\log \gamma_{\rm max}$	$\log \gamma_b$	U_B	$U_{\rm part}$	$(U_{\rm part}/U_B)$	L_k
50.....	0.2	1.05×10^{13}	3.3	5.3	4.8	1.92×10^{-3}	8×10^{-2}	41.5	2.12
1000.....	0.5	1.7×10^{10}	2.8	4.4	3.26	9.95×10^{-3}	400	4.02×10^{4}	10.9

NOTE.—Here δ is the relativistic Doppler factor, B is the magnetic field in gauss, R is the size of the emission region in meters, $\gamma_{\rm min}$, $\gamma_{\rm max}$, and γ_b are the starting, ending, and break Lorentz factors for the primary electron energy spectrum, U_B and $U_{\rm part}$ are energy densities in units of ergs cm^{-3}, and L_k is the minimum kinetic luminosity (defined in § 5) in units of 10^{43} ergs s^{-1}.

break is $t_s = [(4/3)\sigma_{\rm T} c \delta_j (B^2/8\pi m_e c^2)\gamma_b]^{-1} \approx 28$ minutes ($\sigma_{\rm T}$ is the Thomson cross section and m_e is the electron mass). An electron spectrum like the one used here could result from the radiative cooling of a $p = 2$ electron energy spectrum that extends from $\gamma_{\rm min}$ to $\gamma_{\rm max}$, resulting in a spectrum with $p = 2$ and 3 below and above γ_b, respectively.

As shown in Figure 10, both models fail to predict the observed radio fluxes as a consequence of synchrotron self-absorption. We would like to emphasize that we do not regard the discrepancy as a shortcoming of the model. Electrons producing the radio emission cool on much longer timescales, and the radio emission will be dominated by an accumulation of downstream plasma that stopped contributing to the X-ray and TeV emission a long time ago. We could model the radio emission with another emission component (see, e.g., Blazejowski et al. 2005). However, doing so is arbitrary: for a small number of data points we would add an additional model component with many free model parameters.

In Table 2 we list for both models the magnetic field energy density u_B, the energy density in electrons u_e, the ratio $r = u_e/u_B$, and the kinetic luminosity $L_k = \pi R^2 c \Gamma^2 (u_e + u_B)$ for $\Gamma = \delta_j$ (Begelman et al. 1994). The model with a low Doppler factor is closer to equipartition between magnetic field and particles. The kinetic luminosity is similar for the two models, with a high radiative efficiency of the low-δ_j model making up for the stronger boosting of the high-δ_j model.

If taken seriously, the model with $\delta_j = 1000$ would imply that the X-ray and TeV γ-ray emission is produced by an ultrarelativistic particle dominated wind, very close to the supermassive black hole. The fact that seven blazars have been detected at TeV energies seems to argue against extremely relativistic outflows with bulk Lorentz factors Γ on the order of 1000, as isotropic emission would be beamed into an opening angle of Γ^{-1} and would make the observation of the emission unlikely. However, the argument only applies if the jet opening angle is equal or smaller than Γ^{-1}. Having a larger jet opening angle would require a higher total jet luminosity, as some jet segments would not contribute to the observed emission. However, the jet luminosities listed in the table are several orders of magnitude below the Eddington luminosity of a $\sim 10^{8.4}\ M_\odot$ black hole that is suspected to be at the core of Mrk 421 (Barth et al. 2003; Falomo et al. 2002).

We acknowledge an anonymous referee for helpful comments. We acknowledge the technical assistance of E. Roache and J. Melnick. This research is supported by grants from the US Department of Energy, the National Science Foundation, the Smithsonian Institution, by NSERC in Canada, by Science Foundation Ireland, and by PPARC in the UK. H. K. acknowledges support by NASA under grant NAG5-12974.

REFERENCES

Aharonian, F. A. 2000, NewA, 5, 377
———. 2004, Very High Energy Cosmic Gamma Radiation: A Crucial Window on the Extreme Universe (Singapore: World Scientific)
Aharonian, F. A., et al. 1999, A&A, 350, 757
———. 2004, ApJ, 614, 897
———. 2005, A&A, 436, L17
Allen, C. W. 1973, Astrophysical Quantities (New York: Athlone)
Aller, H. D., Aller, M. F., Latimer, G. E., & Hodge, P. E. 1985, ApJS, 59, 513
Baars, J. W. M., Genzel, R., Pauliny-Toth, I. I. K., & Witzel, A. 1977, A&A, 61, 99
Backus, G., & Gilbert, F. 1970, Philos. Trans. R. Soc. London, A, 266, 123
Barth, A. J., Ho, L. C., & Sargent, W. L. W. 2003, ApJ, 583, 134
Bednarek, W. 1997, MNRAS, 285, 69
Bednarek, W., & Protheroe, R. J. 1999, MNRAS, 310, 577
Begelman, M. C., Rees, M. J., & Sikora, M. 1994, ApJ, 429, L57
Blazejowski, M., et al. 2005, ApJ, 630, 130
Böttcher, M., Mause, H., Schlickeiser, R. 1997, A&A, 324, 395
Buckley, J. H., et al. 1996, ApJ, 472, L9
———. 2002, preprint (astro-ph/0201160)
Coppi, P. S. 1999, in Relativistic Jets in AGNs, ed. M. Ostrowski et al. (Krakow: Jagellonian Univ. Press), 333
de la Calle Perez, I., et al. 2003, ApJ, 599, 909
Dickey, J. M., & Lockman, F. J. 1990, ARA&A, 28, 215
Djannati-Atai, A., et al. 1999, A&A, 350, 17
Edelson, R. A., et al. 1988, ApJ, 333, 646
Falcone, A. D., Cui, W., & Finley, J. P. 2004, ApJ, 601, 165
Falomo, R., Kotilainen, J. K., & Treves, A. 2002, ApJ, 569, L35
Fenimore, E. E., Laros, J. G., Klebsadel, R. W., Stockdale, R. E, Kane, S. R. 1982, in AIP Conf. Ser. 77, Gamma-Ray Transients and Related Astrophysical Phenomena, ed. R. E. Lingenfelter, H. S. Hudson, & D. M. Worral (New York: AIP), 201
Finley, J. P., et al. 2001, in Proc. 27th Int. Cosmic Ray Conf. (Hamburg), 2827
Fossati, G., et al. 2000, ApJ, 541, 153
Georganopoulos, M., & Kazanas, D. 2003, ApJ, 594, L27
Ghisellini, G., Tavecchio, F., & Chiaberge, M. 2005, A&A, 432, 401
Ginzburg, V. L., & Syrovatskii, S. I. 1964, Origin of Cosmic Rays (London: Pergamon)
Hartman, R. C., et al. 1992, ApJ, 385, L1
———. 1999, ApJS, 123, 79
Hillas, A. M. 1985, in Proc. 19th Int. Cosmic Ray Conf. (London), 231
Hillas, A. M., et al. 1998, ApJ, 503, 744
Horan, D., & Weekes, T. C. 2004, NewA Rev., 48, 527
Inoue, S., & Takahara, F. 1996, ApJ, 463, 555
Kardashev, N. S. 1962, Soviet Astron., 6, 317
Kataoka, J., Takahashi, T., Makino, F., Inoue, S., Madejski, G. M., Tashiro, M., Urry, C. M., & Kubo, H. 2000, ApJ, 528, 243
Kataoka, J., et al. 1999, ApJ, 514, 138
Kertzman, M. P., & Sembroski, G. H. 1994, Nucl. Instrum. Methods Phys. Res. A, 343, 629
Kino, M., Takahara, F., & Kusunose, M. 2002, ApJ, 564, 97
Kirk, J. G., & Mastichiadis, A. 1999, Astropart. Phys., 11, 45
Kneiske, T. M., Mannheim, K., Hartmann, D. H. 2002, A&A, 386, 1
Konopelko, A., Mastichiadis, A., Kirk, J., De Jager, O. C., & Stecker, F. W. 2003, ApJ, 597, 851
Kosack, K., et al. 2004, ApJ, 608, L97

Krawczynski, H. 2004, NewA Rev., 48, 367
———. 2005, preprint (astro-ph/0508621)
Krawczynski, H., Coppi, P. S., & Aharonian, F. 2002, MNRAS, 336, 721
Krawczynski, H., Coppi, P. S., Maccarone, T., & Aharonian, F. A. 2000, A&A, 353, 97
Krawczynski, H., Hughes, S. B., & Horan, D. 2004, ApJ, 601, 151
Krawczynski, H., et al. 2001, ApJ, 559, 187
Krennrich, F., & Dwek, E. 2003, in Proc. 28th Int. Cosmic Ray Conf. (Trukuba), 2667
Krennrich, F., et al. 1999, ApJ, 511, 149
———. 2002, ApJ, 575, L9
Levine, A. M., et al. 1996, ApJ, 469, L33
Li, T., & Ma, Y. 1983, ApJ, 272, 317
Loredo, T. J., & Epstein, R. I. 1989, ApJ, 336, 896
Mannheim, K. 1998, Science, 279, 684
Mastichiadis, A., & Kirk, J. G. 1997, A&A, 320, 19
Mücke, A., Protheroe, R. J., Engel, R., Rachen, J. P., & Stanev, T. 2003, Astropart. Phys., 18, 593
Mirzoyan, R., et al. 1994, Nucl. Instrum. Methods Phys. Res., A351, 513
Ong, R. A., 2003, in The Universe Viewed in Gamma-Rays, ed. R. Enomoto, M. Mori, & S. Yanagita (Tokyo: Universal Academy), 587
Pacholczyk, A. G. 1970, Radio Astrophysics (San Francisco: Freeman)
Petry, D., et al. 2002, ApJ, 580, 104
Piner, B. G., & Edwards, P. G. 2005, ApJ, 622, 168
Piron, F. 2001, preprint (astro-ph/0106210)
Pohl, M., & Schlickeiser, R. 2000, A&A, 354, 395
Press, W. H., Teukolsky, S. A., Vetterling, W. T., & Flannery, B. P. 1992, Numerical Recipes in C (2nd ed.; Cambridge: Cambridge Univ. Press), 694
Punch, M., & Fegan, D. J. 1991, in AIP Conf. Proc. 220, High Energy Gamma Ray Astronomy, ed. J. Matthews (New York: AIP), 321
Punch, M., et al. 1991, in Proc. 22nd Int. Cosmic Ray Conf. (Dublin), 464
———. 1992, Nature, 358, 477
Rauterberg, G. 1995, in Proc. 24th Int. Cosmic Ray Conf. (Rome), 460
Reynolds, P. T., et al. 1993, ApJ, 404, 206
Sambruna, R. M., et al. 2000, ApJ, 538, 127
Sikora, M., & Madejski, G. 2001, in AIP Conf. Ser. 558, High Energy Gamma-Ray Astronomy, ed. F. A. Aharonian & H. J. Völk (New York: AIP), 275
Sokolov, A., Marscher, A., & McHardy, I. M. 2004, ApJ, 613, 725
Syrovatskii, S. I. 1959, Soviet Astron., 3, 22
Takahashi, T., et al. 1996, ApJ, 470, L89
———. 2000, ApJ, 542, L105
Tanihata, C., et al. 2001, ApJ, 563, 569
Tavecchio, F. 2006, in Proc. 10th Marcel Grossman Meeting on General Relativity, in press (astro-ph/0401590)
Villata, M., Raiteri, C. M., Lanteri, L., Sobrito, G., & Cavallone, M. 1998, A&AS, 130, 305
Weekes, T. C. 1996, Space Sci. Rev., 75, 1
———. 2003, Very High Energy Gamma-Ray Astronomy (Bristol: IOP)
Zweerink, J. A., et al. 1997, ApJ, 490, L141